[8] P. J. B. Clarricoats and K. B. Chan, "Electromagnetic wave propagation along radially inhomogeneous dielectric cylinders," *Electron. Lett.*, vol. 6, pp. 694–695, 1970.
[9] Y. Suematsu and K. Furuya, "Propagation mode and scattering loss of a two-dimensional dielectric waveguide with gradual distribution of refractive index," *IEEE Trans. Microwave Theory Tech.*, vol. MTT-20, pp. 524–531, Aug. 1972.
[10] K. F. Casey, "Radiation from a line source near an inhomogeneous layer," *IEEE Trans. Antennas Propagat.*, vol. AP-21, pp. 640–648, Sept. 1973.
[11] D. Marcuse, "TE modes of graded-index slab waveguides," *IEEE J. Quantum Electron.*, vol. QE-9, pp. 1000–1006, Oct. 1973.
[12] M. Godart, "An iterative method for the solution of eigenvalue problems," *Math. Comput.*, vol. 20, pp. 399–406, 1966.
[13] E. F. Kuester and D. C. Chang, "Modal and coupling characteristics of inhomogeneous dielectric slab waveguides—Part I: Lossless slabs," Univ. Colorado, Boulder, Sci. Rep. 1, Air Force Contract AFOSR-72-2417, 1973.
[14] M. R. Scott *et al.*, "Invariant imbedding and the calculation of eigenvalues for Sturm-Liouville systems," *Computing*, vol. 4, pp. 10–23, 1969.
[15] R. J. Garbacz, "Electromagnetic scattering from radially inhomogeneous spheres," *Proc. IRE* (Corresp.), vol. 50, p. 1837, Aug. 1962.
[16] G. Millington, "Ricatti form of the wave equation," *Electron. Lett.*, vol. 1, pp. 184–185, 1965.
[17] R. Bellman and R. Kalaba, "Functional equations, wave propagation, and invariant imbedding," *J. Math. Mech.*, vol. 8, pp. 683–704, 1959.
[18] L. F. Shampine and H. A. Watts, "Computing error estimates for Runge-Kutta methods," *Math. Comput.*, vol. 25, pp. 445–455, 1971.
[19] D. Gloge, A. R. Tynes, M. A. Duguay, and J. W. Hansen, "Picosecond pulse distortion in optical fibers," *IEEE J. Quantum Electron.* (*Special Issue on 1971 IEEE/OSA Conference on Laser Engineering and Applications: Part II of Two Parts*), vol. QE-8, pp. 217–221, Feb. 1972.
[20] E. F. Kuester and D. C. Chang, "Modal and coupling characteristics of inhomogeneous dielectric slab waveguides—Part II: Lossy slabs and pulse dispersion," Univ. Colorado, Boulder, Sci. Rep. 7, Air Force Contract AFOSR-72-2417, 1974.
[21] J. J. Burke, "Propagation constants of resonant waves on homogeneous isotropic slab waveguides," *Appl. Opt.*, vol. 9, pp. 2444–2452, 1970.
[22] J. G. Doidge, "Investigation of the theory of a thin film optical transmission line," Autonetics Div., NAA, Anaheim, Calif., Sci. Rep. 1, Air Force Contract AF 49(638)-1504, 1966.
[23] G. J. Gabriel and M. E. Brodwin, "The solution of guided waves in inhomogeneous anisotropic media by perturbation and variational methods," *IEEE Trans. Microwave Theory Tech.*, vol. MTT-13, pp. 364–370, May 1965.
[24] F. P. Kapron and D. B. Keck, "Pulse transmission through a dielectric optical waveguide," *Appl. Opt.*, vol. 10, pp. 1519–1523, 1971.
[25] C. G. B. Garrett and A. E. McCumber, "Propagation of a Gaussian light pulse through an anomalous dispersion medium," *Phys. Rev. A*, vol. 1, pp. 305–313, 1970.
[26] P. C. Clemmow, *The Plane Wave Spectrum Representation of Electromagnetic Fields*. London, England: Pergamon, 1966, p. 76.
[27] S. Kawakami and S. Nishida, "Anomalous dispersion of new doubly clad optical fibre," *Electron. Lett.*, vol. 10, pp. 38–40, 1974.
[28] D. Gloge, "Dispersion in weakly guiding fibers," *Appl. Opt.*, vol. 10, pp. 2442–2445, 1971.
[29] E. F. Kuester and D. C. Chang, "Single-mode pulse dispersion in optical waveguides," to be published.
[30] D. Marcuse, *Light Transmission Optics*. New York: Van Nostrand Reinhold, 1972, ch. 6.

Propagation Effects in Optical Fibers

DETLEF GLOGE, MEMBER, IEEE

(Invited Paper)

***Abstract*—The round dielectric waveguide exhibits a surprising variety of characteristics that are not accurately inferable from the slab model. The forceful effort of recent years has grately extended the knowledge of these structures and added new and exciting modifications. An attempt to unify these results in a simplified picture is made. Specific phenomena relevant to optical fiber design and fabrication are then brought into focus. Some of the problems discussed are cross sectional loss variations, various core index profiles and the tolerances required in their preparation, the necessary cladding thickness, directional changes, and sources of mode coupling affecting signal distortion and loss.**

I. INTRODUCTION

THE LAST few years have seen a rapid increase both in technological know-how and theoretical understanding of optical fibers and, along with it, a new variety of fiber structures. At the same time, the issue of material loss, which had barred fibers from the communications field longer than necessary, was so convincingly solved that other aspects are now becoming a prime concern of optical communications research. This then seems to be a good time to take stock, to organize the knowledge gained, and to assess the available options. Accordingly, a great number of review articles have appeared in a rapid sequence all over the world. To name only the most recent in the order of their appearance, there is an article by Maurer [1] addressed mainly to the technology of fiber preparation. *Opto-Electronics* devoted its July and September issues of 1973 to the subject of fiber optics featuring reviews of the state of the art in Britain [2] and Germany [3]. An article by Ohnesorge [4] advanced some of the less conventional ideas of communication systems application for optical fibers. Miller *et al.* [5] have prepared a very comprehensive review of the current knowledge relating it to potential applications in the conventional communications network. The quite different though equally immediate potential of fibers for military applications becomes apparent in an article [6] which appeared in this TRANSACTIONS in December, 1973. The conventional technology of fiber bundles [7] seems to be more

Manuscript received March 27, 1974; revised August 15, 1974.
The author is with the Crawford Hill Laboratory, Bell Laboratories, Holmdel, N. J.

readily applicable in this case, where multiterminal information transfer over short distances on board aircraft or ship is the objective. To complete our "review of the reviews," we should mention a 6-page summary of the state of the art [8], interesting for those looking for a concise overview, and, of course, some of the textbooks available on the theory of dielectric wave guidance [9]–[11]. It is quite likely that review articles on optical fibers will continue to appear within similar or even shorter intervals. An English-language paper on the very extensive and successful work in Japan [12], for example, would be quite welcome. On the other hand, those interested in the field are by now quite well informed about the history and breakthrough of communication-oriented fiber optics and can find more than 300 references on the details in the reviews cited earlier.

Rather than adding to this list, I wish to narrow the objectives of this paper in an attempt to present a concise and unified picture of the propagation characteristics of the round dielectric waveguide both in its ideal and its imperfect state, in order to provide some simple results relevant to design and systems questions in optical transmission applications. Many of these results deviate sufficiently from the well-known characteristics of the two-dimensional dielectric-film model to arouse some caution as to the validity of the usual extrapolations of film concepts to the fiber description. One of the objectives of this article is, therefore, a closer look at the limits of our knowledge of the round dielectric structure and the identification of areas where further investigations are necessary. In line with these objectives, references are cited merely to direct the reader to additional material on a given subject matter and are not necessarily the first or only publications on the subject.

We begin in Section II with a discussion of the guidance concepts governing the round dielectric waveguide. Aside from the classical core-cladding structure, this includes cylindrical graded-index profiles and slab-supported guides. Section III takes a look at realistic fibers in a practical environment and attempts to incorporate the influence of cross sectional loss variations, finite cladding thickness, directional changes, and random imperfections in the laws of propagation. The emphasis is on measurable variables and measured results. The dispersive effect of the material and the waveguide, delay between fiber modes, and the resulting signal distortion are the subject of Section IV.

II. GUIDANCE PRINCIPLES

Trapped or lossless propagation of light in dielectric waveguides relates to idealized structures which are straight and unperturbed in propagation direction, have unperturbed surroundings (infinitely thick cladding) and are made from lossless materials. This is the structure we discuss in this section, confident that slight modifications will later suffice to adapt the results to practical conditions; perturbation methods to achieve this are discussed in the next section. The classical clad glass fiber [7] traps light by total internal reflection at the core boundaries where the index drops to the slightly lower cladding value. Modern structures like the graded-index fiber whose index decreases gradually outward from the axis employ a continuous focussing process to achieve trapping, which can be considered as a kind of distributed internal reflection [13]. Propagation in the single-material fiber [14] is not characterized by an index change at all, but solely by the cross sectional configuration. Whatever the underlying principle of guidance, all structures can be designed to support one or many trapped modes of propagation. Beginning with the classical clad structure, we shall discuss its single-mode configuration in greater detail, hoping that this will aid in the understanding of the other two.

The round clad fiber is one of the few dielectric waveguide structures, for which Maxwell's equations have rigorous (though fairly unwieldy) solutions and these have been discussed in many places [9], [10]. The very existence of such solutions has probably kept theorists from searching for simplifying approximations even after such approximations were found, and recognized as useful, in the case of the parabolically graded index profile (see, for example [15]). The approximations recognize the fact that, ultimately for technological reasons, the change from the core index n_1 to the cladding index n_2 is typically small. In other words,

$$n_2 = n_1(1 - \Delta) \tag{1}$$

and $\Delta \ll 1$. Under these conditions, field solutions can be found both for the flat and the graded core index profile, which are essentially transverse electromagnetic and linearly polarized [15]–[17]. Strictly speaking, all these solutions (except for the fundamental) are superpositions of more complicated field solutions that appear degenerate in these approximations, but in reality break apart upon propagation over long distances as a result of small differences in the propagation constants. The approximations are completely satisfactory, however, in predicting the modal power distributions and group velocities; this is essentially what is needed in fiber-optical communication systems, which, for the time being, are restricted to direct (power) modulation and detection for economical reasons.

In the case of the classical fiber structure, which has an abrupt index step at the core-cladding boundary, the approximation ignores essentially the slight difference (of order Δ^2) in the matching conditions for the electric and magnetic field components tangential to that boundary. As a result, the boundary conditions simply require continuity of all transverse field amplitudes and their radial derivatives through the boundary. In a cylindrical structure, these conditions can be met by the well-known trial solution

$$\boldsymbol{E}(r,\phi) = E(a) \begin{cases} J_l(ur/a)/J_l(u) & r < a \\ K_l(wr/a)/K_l(w) & r > a \end{cases} \cos l\phi, \tag{2}$$

where $k = 2\pi/\lambda$ is the free-space wave number, a the core radius, and $E(a)$ the maximum field amplitude at the interface; u and w are a pair of parameters, whose mutual interrelation is determined by the matching conditions

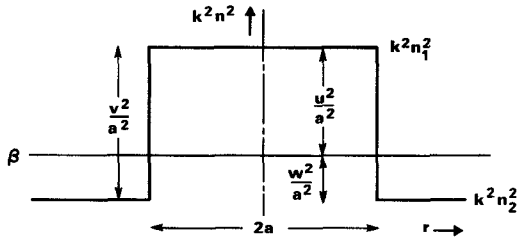

Fig. 1. Dielectric profile of the single-mode fiber with uniform core index.

[16], [17]. How u and w relate to the propagation constant β and the structural parameter v (usually called the v-value) is evident from the dielectric profile sketched in Fig. 1. We find

$$v = (u^2 + w^2)^{1/2} = ak(n_1^2 - n_2^2)^{1/2} \approx akn_1(2\Delta)^{1/2} \quad (3)$$

and

$$\beta^2/k^2 = n_2^2 + (n_1^2 - n_2^2)w^2/v^2. \quad (4)$$

In general, the problem of characterizing the modes of a certain fiber can be approached in the following way: the measurement of a, Δ, and the wavelength of operation determines v. The parameters u and w then result from (3) and the (transcendental) "characteristic equation" derived from the matching conditions [16], [17]. Equation (4) finally permits the computation of β. For many technical problems, u, w, or β are of little direct use, except as a basis for calculating the more important mode power and group velocity relations. For example, the question of how bulk loss differences in core and cladding affect the mode loss requires some knowledge of the power distribution in core and cladding. In the classical fiber structure, the mode power and group velocity relations can be derived from an auxiliary parameter [17], [11]

$$j_l = -\frac{J_l^2(u)}{J_{l+1}(u)J_{l-1}(u)}. \quad (5)$$

If P is the total power in a certain mode and P_1 and P_2 are the power fractions in core and cladding, we find [17]

$$\frac{P_1}{P} = 1 - \frac{P_2}{P} = (1 + j_l)w^2/v^2. \quad (6)$$

The power density at the core-cladding interface, averaged over the circumference, is

$$p(a) = \frac{P}{\pi a^2} j_l w^2/v^2. \quad (7)$$

The density $p(a)$ determines the amount of mode loss caused by imperfections in the interface. The group velocity relations of interest are discussed in Section IV.

This outline would be of little help to the reader without some knowledge of how to obtain u or w. Before this is discussed, we must take a closer look at situations of practical interest and the numbers of modes involved in these cases. The approximate theory, on which our discussions are based, stipulates that the number of independent field solutions (degenerate mode groups) is equal to the number of zeros of all Bessel functions J_l which are smaller than v, plus the fundamental solution [16], [17]. If $v < 2.4$, only the fundamental mode propagates. This mode has the transverse field distribution $J_0(ur/a)$ in the core. The cladding field decays monotonically with the distance from the interface; it reaches farther and farther into the cladding as v decreases. A theory which considers the cladding thickness as unlimited finds this mode to be trapped even as v approaches zero.

There are two distinctly different operating conditions for fibers used in transmission systems: single-mode and multimode operation. The former avoids the signal-impairing effect of mode delay differences and therefore provides the ultimate in transmission bandwidth. For this reason, the single-mode fiber has a definite potential for wide-band optical communication; it is likely to gain in importance once sources become available [18] that have sufficient spatial coherence to excite the one mode of the single-mode fiber efficiently. On the other hand, single-mode operation limits the core diameter and the index difference as well as the tolerances acceptable for these two parameters, a fact which may complicate large-scale fabrication and field splicing of such fibers. Secondly, and maybe more importantly, since the single-mode fiber accepts only the equivalent of one radiation mode from any source, it is practically useless in combination with incoherent sources (luminescent diodes) and deficient, if the source is multimode. For all these reasons and because recent fiber art has devised schemes of alleviating the signal impairing effect of mode delay differences in multimode fibers, multimode operation is at least of equal importance. Typically, such fibers are designed to support a great number of modes in order to fully bring their advantages to bear.

Coming back now to the computation of the parameters u or w from v, we distinguish the two cases of single-mode and multimode operation. As we shall see, the second case allows a rather summary treatment of all modes yielding closed-form approximations of satisfactory accuracy. Rather than enumerating similar approximations valid in specific regions of the single-mode regime, we simply plot here all important parameters characterizing the fundamental mode in a way that allows an accurate reading everywhere. For this reason, the ordinate of Fig. 2 is chosen linear around unity and logarithmic below. Plotted along the abscissa is the v-value in the region between $v = 0.6$ and 2.4, which covers the single-mode regime of interest. In addition to the parameters u and w, we have plotted w^2/v^2, which determines β according to (4), j_0w^2/v^2, which is proportional to $p(a)$ of (7), and $(1 + j_0)w^2/v^2$, which determines the power distribution (6). Accordingly, P_1/P can be read off the left side and P_2/P off the right side of Fig. 2.

Although, theoretically, the fundamental has no cutoff as v decreases and hence propagates even at lowest frequencies, it is obvious from Fig. 2 that the power contained by the core is only 0.1 percent at $v = 0.6$ and decreases rapidly for lower v, making effective guidance

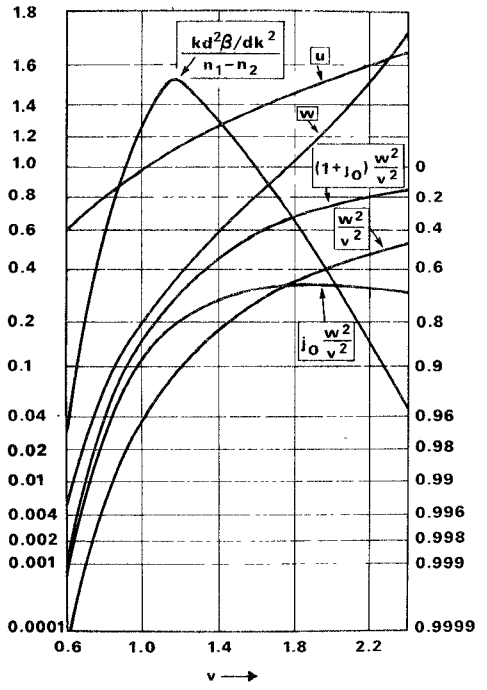

Fig. 2. Various characteristics of the fundamental mode in the step-index fiber plotted versus the v-value.

below $v = 0.6$ virtually impossible. More interesting than the lower bound is the region towards large v, because, at optical wavelengths, the objective is in making the core radius a and hence v as large as possible, to alleviate fabrication and splicing tolerances. A safe operating point may be $v = 2$. Any remaining effort in maximizing a is limited to a reduction of Δ. The parameter Δ, on the other hand, must at least be of the order of 0.3 percent if excessive bending loss is to be avoided; this condition is explained by (41) of Section III. As a result, we find with the help of (3) that the core diameter of the single-mode fiber can measure 5 to 6 wavelengths at the most.

Plots similar to Fig. 2 can be produced for all modes of the classical fiber structure when the region of v is extended to larger values [17]. Such detailed knowledge of every one of the hundreds of modes propagating in typical multimode fibers can be rather confusing. On the other hand, one arrives at very satisfactory closed-form expressions of general validity for all but the very lowest order modes, if one makes use of the Debye approximations for the Bessel functions [19]. Although these approximations are rather simple and straightforward as far as the mathematical side of the problem is concerned, a direct derivation from physical principles has several side benefits. One is an effortless association of modes with rays [20], the other is an easy extension of these principles to fibers with a nonuniform core index, which will be of use later on. The direct derivation uses the method of Wentzel, Kramers, Brillouin, and Jeffreys (WKBJ) modified to apply to cylindrical structures [21], [22]. This approach is outlined in the Appendix. The following more casual argument is based on the same ideas but requires less mathematics [23].

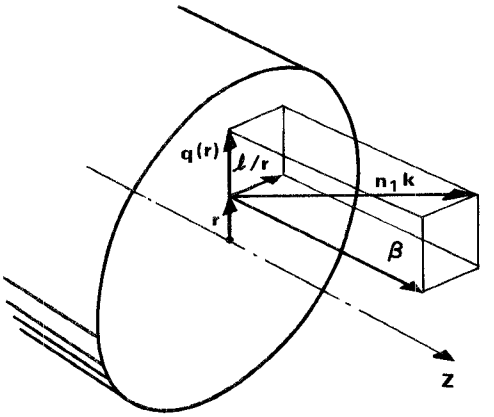

Fig. 3. Wave vector diagram in the propagation region of a multimode fiber.

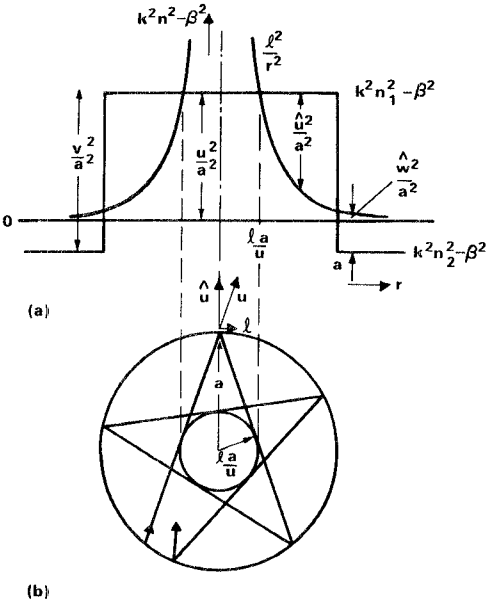

Fig. 4. (a) Dielectric profile of the classical fiber structure (uniform core index) showing squared magnitudes of vector components for azimuthal mode order l.

We assume the existence of locally plane waves in the core guidance region. Fig. 3 shows a decomposition of the local wave vector (pertaining to a given mode) into its components in the cylindrical coordinate system (r, ϕ, z). The axial component is the propagation constant β of the mode. The azimuthal periodicity indicated by $\cos l\phi$ in (2) results in a ϕ-component l/r at r. Since the magnitude of the wave vector is nk, the radial component becomes

$$q(r) = (k^2n^2 - \beta^2 - l^2/r^2)^{1/2} \tag{8}$$

with $n = n_1$ in the core and $n = n_2$ in the cladding. Fig. 4 is a plot of a dielectric profile similar to Fig. 1, showing the square magnitudes of the various components as a function of the radius. Within the region $la/u < r < a$, in which q is real, we introduce a parameter

$$\hat{u} = qa = (u^2 - l^2a^2/r^2)^{1/2}. \tag{9}$$

This region represents the core area, in which a periodic field solution exists. Outside of this region, both in the core and in the cladding, the radial component becomes

imaginary, causing the mode field to decay monotonically with the distance from the boundaries. The decay parameter in the cladding is

$$\hat{w} = (w^2 + l^2a^2/r^2)^{1/2}. \tag{10}$$

The cylindrical surface of radius la/u in the core represents a caustic [20] for rays which travel within the region $la/u < r < a$ and have the direction of the local wave vector. A cross sectional projection of one of these rays is shown in Fig. 3(b). The entire group represents the "congruence" of rays [20] associated with the mode under discussion. Before we define this mode more fully, let us digress briefly to take a closer look at the ray picture. The angle which all rays of a congruence form with the axis obeys the relation

$$\sin\theta = u/akn_1. \tag{11}$$

When the rays leave the fiber end face into air, $\sin\theta$ increases to

$$\sin\Theta = u/ak \tag{12}$$

as a result of refraction. For small Θ, if we were to set up a screen perpendicular to the axis at a distance ak mm away from the end face, all these rays would impinge on the screen approximately at a distance u mm from the axis. In typical multimode fibers, ak may be of the order of 100 and u varies between 0 and v, the latter being of the order of 30. In accordance with lens optics definitions the product of the refractive index and the sine of the maximum ray angle, that is,

$$n_1 \sin\theta_{max} = v/ak = (n_1^2 - n_2^2)^{1/2} \approx n_1(2\Delta)^{1/2} \tag{13}$$

is called the numerical aperture of the fiber.

A complete identification of the modes of the cylindrical structure requires two mode numbers: the azimuthal order number discussed earlier and a meridional order number m, which identifies the number of field maxima of the radial field solution (this count includes the maximum at $r = 0$ for $l = 0$). The WKBJ approximation for m is obtained from a count of the number of half periods comprised within the radial phase change between the caustic and the interface. This results in the relation

$$m\pi = \int_{l/u}^{1} \hat{u}\, d\rho \tag{14}$$

with $\rho = r/a$. A rigorous and more accurate derivation of this relationship can be found in the Appendix. However, (14) gives usually a satisfactory description of the modes of a typical multimode fiber. In the case of the classical index profile, we can solve (14) after inserting (9) and obtain

$$m = (1/\pi)[(u^2 - l^2)^{1/2} - l \arccos(l/u)]. \tag{15}$$

Fig. 5 illustrates this relation for different ratios u/v. Modes are marked in this plot by a uniform raster of spots of density $1/v^2$ (see upper right of Fig. 5). Each spot to the left of the line $u/v = 1$ represents a degenerate quadruplet of trapped modes of different polarization or orientation. There are no spots along the ordinate since $m = 1,2,\cdots$; spots falling on the abscissa ($l = 0$) represent doublets [11]. If $v \gg 1$, as for typical multimode fibers, we can count the total number of modes simply by integrating (15) with respect to l. The result is the mode volume

$$M = 4\int_0^v m(l)\, dl = v^2/2. \tag{16}$$

Given a certain mode (m,l), Fig. 5 provides the u-value of that mode. The characteristic ray (or group of rays)

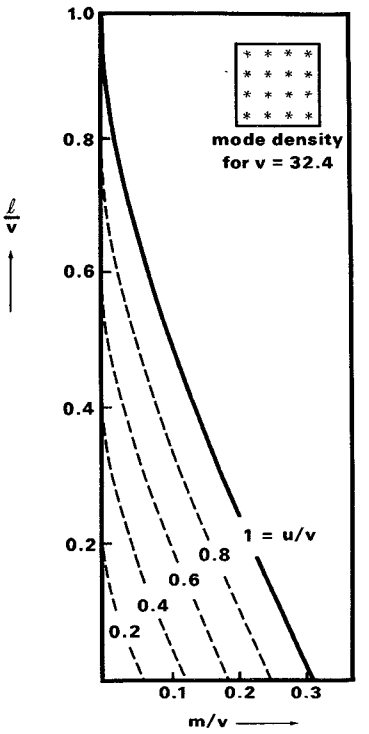

Fig. 5. Plot of mode number l versus m for different parameters u, all normalized with respect to the v-value; density of modes is $1/v^2$ (see upper right); all spots to left of $u/v = 1$ designate degenerate groups of trapped modes.

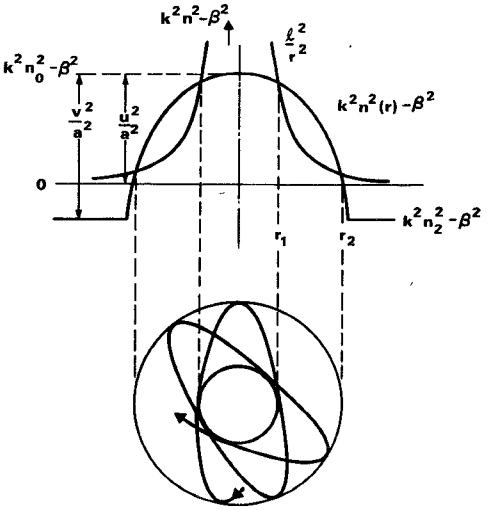

Fig. 6. (a) Dielectric profile of a graded index fiber showing caustics for mode characterized by u, l. (b) Cross sectional projection of a ray characterizing above mode.

of that mode is then defined by (11) and the caustic at $r = al/u$. Equation (4) and the relation $w^2 = v^2 - u^2$ yield the propagation constant β. As for the power distribution, a more accurate match of the field solutions (A9) at the interface is necessary to obtain the approximation

$$j_l \approx \frac{u^2}{w^2}\left[1 - \frac{1}{h + (w^2 + l^2)^{1/2}}\right] \tag{17}$$

with $h = 1$ for $l = 0$ and $h = 0$ for $l \neq 0$. By using this relation in (6), the cladding power becomes

$$P_2 = \frac{Pu^2/v^2}{h + (w^2 + l^2)^{1/2}}. \tag{18}$$

Note, that $P_2 = P/(h + l)$ at cutoff, where $u = v$ and $w = 0$. Thus, contrary to the mode behavior in the slab (or for $l = 0, 1$ in the fiber), a good fraction of most fiber modes is concentrated in the core even at cutoff. This is a result of the fact that the cladding field solution (A9) decreases as r^{-l} at cutoff, where $\hat{w} = l/r$.

The convenience of detection and measurement in the optical far-field renders the modal far-field distribution often more important than the mode field itself. We recall that the exit angle Θ of a ray characterized by m and l obeys the relation (12) and is only a function of u and not explicitely of m and l. We can therefore infer that, as $ka \to \infty$, the far-field radiation of all modes characterized by u converges on a cone with half-apex angle Θ. A different, though somewhat more general, interpretation of the same relationship stipulates that the power $dP(u)$ of all modes falling between two lines characterized by u and $u + du$ in Fig. 5 can be collected in a ring of radius u and width du on a screen a distance ak away from the fiber end (measure u and ak in millimeters, say).

Fig. 6 depicts the dielectric profile and a ray projection in the case of a graded core index profile. The area of periodic field solutions is now limited by two caustics. Rays characterized by u exit at the angle Θ only, if they leave the guide exactly from the center (only possible for meriodional rays). All other exit positions of rays characterized by u lead to exit angles smaller than $\Theta(u)$. Accordingly, the far-field relations for $ka \to \infty$ in the graded-index case are not as simple as in the case of the uniform core. A straightforward modification of (14) results in the characteristic integral

$$m = \frac{1}{\pi}\int_{r_1}^{r_2} [k^2 n^2(r) - \beta^2 - l^2/r^2]^{1/2}\, dr \tag{19}$$

where we have again neglected a small term additive to m. A class of profiles of particular interest has the form

$$n(r) = n_0 \begin{Bmatrix} (1 - 2\Delta\rho^g)^{1/2}, & \rho < 1 \\ (1 - 2\Delta)^{1/2}, & \rho > 1 \end{Bmatrix} \quad g > 1. \tag{20}$$

It includes the classical fiber with uniform core discussed so far ($g \to \infty$) as well as the parabolic index distribution ($g = 2$); the latter is important because it provides an effective equalization of the modal group velocities [13]. We return to the discussion of this effect in Section IV.

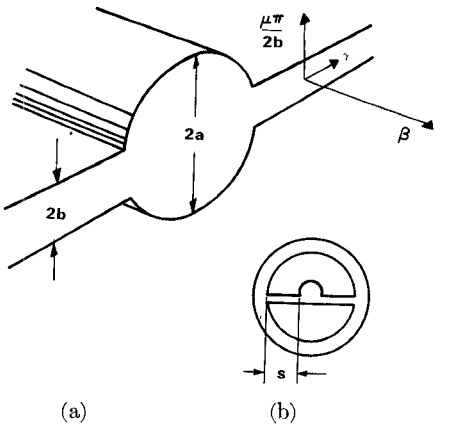

Fig. 7. (a) Sketch of single-material fiber showing vector diagram in membrane. (b) Typical cross section showing membrane length s.

An exact solution of (19) is not known, but I have found the approximation

$$l + 4\left(\frac{2}{2+g}\right)^{2/g} m = \left(\frac{g}{g+2}\right)^{1/2}\left(\frac{2}{g+2}\right)^{1/g} u\left(\frac{u}{v}\right)^{2/g} \tag{21}$$

very satisfactory. It is exact for $g = 2$ and very good as long as g is not too large. The maximum error results for $g \to \infty$ and can be inferred from a comparison with (15). An integration of (21) similar to (16) yields the mode volume

$$M_g = \frac{1}{2}\frac{gv^2}{g+2} \tag{22}$$

which can be shown [23] to be exact for all g within the limits of the approximations that apply to (19). As (22) shows, the mode volume of the graded profile is typically less than that of the uniform core when both have the same total index difference. Parabolic grading, for example yields $M_2 = M_\infty/2$.

The fiber configuration of Fig. 7 permits the trapped propagation of a desired number of modes in a core which is suspended between two membranes made of the same material as the core [14]. Although there is no index change between the core and the membranes, the latter have a function similar to that of the cladding in previous configurations. In line with the idealizations applied to those, we assume for the time being that the membranes extend to infinity to both sides of the core. To understand the function of the membrane, consider the wave vector diagram of an arbitrary (plane) wave field in the membrane (see Fig. 7) [24]. The large index change between the membrane and the surrounding air enforces a transverse wavenumber of a magnitude close to $\mu\pi/2b$, where $\mu = 1,2,\cdots$ and b is the half width of the membrane. The vector summation yields

$$k^2 n_1^2 = \beta^2 + \left(\frac{\mu\pi}{2b}\right)^2 + \gamma^2. \tag{23}$$

If the membrane field is part of a core mode, β is the propagation constant of that mode and hence, with the notation of Fig. 1,

$$\frac{u^2}{a^2} = \left(\frac{\mu\pi}{2b}\right)^2 + \gamma^2. \tag{24}$$

Trapping of core modes requires that all field solutions are of the evanescent type along the membranes and hence γ must be imaginary even for the smallest μ, that is, $\mu = 1$. Consequently, $u/a \leq \pi/2b$, where the equality denotes cutoff for the mode characterized by u. Since per definition $u = v$ at cutoff, we can define an effective v-value of this fiber configuration of the form

$$v_e = \pi a/2b. \tag{25}$$

By using v_e instead of v in (3) and all subsequent equations as well as in Figs. 2 and 5 we obtain essentially all mode characteristics of this fiber structure, including the conditions for single- or multimode operation.

III. PROPAGATION LOSSES

Mode attenuation results first of all from the dissipative and scattering loss of the core and cladding materials and the interface between the two. Secondly, loss can be caused by the finite cladding width and the (sometimes intentionally) lossy jacket around the cladding. Thirdly, a radiation loss is suffered by modes which are not fully trapped. All three sources of loss usually affect different modes differently. Even small loss differences can cause virtual extinction of some modes in comparison to others, if the fiber is sufficiently long. In general, coupling of modes as a result of perturbations along the fiber balances the effect of loss differences by continuously transferring power into modes otherwise lost. Ultimately, this transfer causes a loss in all modes.

Let us first ignore the complicating influence of coupling. This assumption seems quite relevant to potential communications applications, since careful preparation and handling of fibers has been shown to reduce coupling to negligible amounts even in long fiber lengths [25]. Under these conditions a loss of, say, α_1 dB/km in the core and α_2 dB/km in the cladding produces a mode loss

$$\alpha_I(m,l) = \alpha_1 P_1/P + \alpha_2 P_2/P. \tag{26}$$

with P_1 and P_2 from (6). If we ignore the case $l = 1$, we have $h = 0$ in (17) and

$$\alpha_I = \alpha_1 + (\alpha_2 - \alpha_1)\frac{u^2}{v^2}(w^2 + l^2)^{-1/2}. \tag{27}$$

for the classical step-index profile. Fig. 8 is a plot similar to Fig. 5 showing lines of constant α_I. In the case of large v, the loss of few modes exceeds α_1 even if α_2 is large. Similar modal loss coefficients can be derived with the help of (7), if a source of loss exists in the interface between core and cladding.

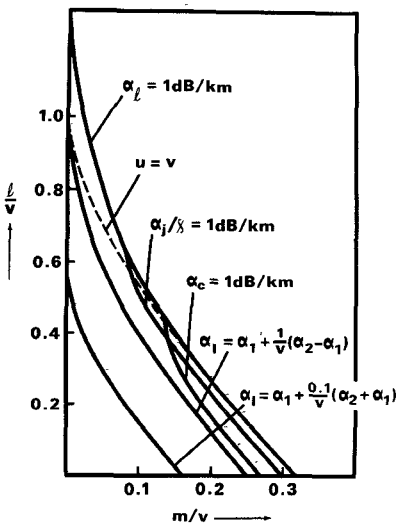

Fig. 8. Same plot as Fig. 5 (broken line is boundary for trapped modes); solid lines are lines of constant loss for various loss phenomena: α_l—leakage loss, α_j/χ—jacket loss, α_c—curvature loss, α_I—loss as a result of cross sectional loss variation of the form (26).

A graded profile is generally obtained by adding or exchanging one or more components in the host glass. It is likely that the additive causes a certain excess loss or, in the case of an exchange, that the loss of one component is different from that of the other. In either case, the loss variation is likely to follow the index variation so that the loss at a distance r from the axis becomes

$$\alpha(r) = \alpha_0 + (\alpha_2 - \alpha_0)\frac{n_0^2 - n^2(r)}{n_0^2 - n_2^2}. \tag{28}$$

The loss suffered by a given mode is in this case

$$\alpha_{II} = \int_0^\infty \alpha(r)p(r)r\,dr \Big/ \int_0^\infty p(r)r\,dr \tag{29}$$

where $p(r)$ is the power density of that mode at r. To solve (29) we use the relation [26]

$$\frac{\beta}{k}\frac{d\beta}{dk} = \int_0^\infty n^2(r)p(r)r\,dr \Big/ \int_0^\infty p(r)r\,dr \tag{30}$$

and $d\beta/dk = ct(u)$ from (60) of Section IV. We obtain

$$\alpha_{II} = \alpha_0 + (\alpha_2 - \alpha_0)\frac{2}{g+2}\frac{u^2}{v^2}. \tag{31}$$

Note that (31) does not converge into (27) for $g \to \infty$, but yields $\alpha_{II} = \alpha_0$. This is so because (31) is based on the assumption of negligible evanescent fields, which was introduced to obtain (19). This approximating assumption is valid and useful in cases when both index and loss vary within the regions of propagating field solutions (between the two caustics), because the different extent of these regions for different modes is then likely to be the overriding influence in causing loss differences among the modes. This effect disappears of course for $g \to \infty$,

and the second-order effects expressed by (27) are then the predominant source of loss differences.

Although assumed infinitely thick in Section II, the fiber cladding measures typically only tens of micrometers in thickness and is covered by a lossy jacket to avoid crosstalk to other fibers. The resulting perturbation of the mode fields of Section II is nevertheless small because of the rapid cladding field decay of almost all modes. For this reason, the power loss can be obtained in good approximation from the unperturbed mode field with the help of the matching conditions at the jacket interface [27]. If the (complex) jacket index is n_j and its real part is not too different from the cladding index, the ratio between the radial and the axial power flow at the interface becomes [27]

$$\chi = \mathrm{Re}\,[(kn_j/\beta)^2 - 1]^{1/2}. \tag{32}$$

Assuming a cladding thickness s, we can relate the power loss α_j to the averaged power density $p(a + s)$ at the jacket interface by integrating around the circumference and dividing by the total mode power P. The result is

$$\alpha_j = 4.34\pi(a + s)\chi p(a + s)/P \text{ in dB}. \tag{33}$$

After inserting (7) and (A9), we have

$$\alpha_j = \frac{4.34}{a}\chi\frac{\hat{w}(a)}{\hat{w}(a + s)}j_l\frac{w^2}{v^2}\exp\left(-2\int_a^{a+s}\hat{w}\,dr/a\right) \tag{34}$$

with $\hat{w}$ from (10) in the case of the step index profile. If $l = 0$,

$$s = \frac{a}{2w}\ln\,(4.34\chi j_l w^2/v^2 a\alpha_j). \tag{35}$$

In the case of the single-mode fiber operating at $v = 2$, we find most parameters appearing in (35) from Fig. 2 and obtain $s = 8a$ for $\alpha_j/\chi = 1$ dB/km, in good agreement with results of [27]. The great variety of potential jackets makes it difficult to find a representative value for χ. It may be of the order of unity or smaller. On the other hand, it is evident from (35) that s is not very sensitive to the ratio α_j/χ.

The fairly complicated rigorous solution of (34) for $l \neq 0$ is omitted here. The line $\alpha_j/\chi = 1$ *dB/km* in Fig. 8 depicts the result for the specific example:

core radius a	$= 25\ \mu$m
cladding thickness s	$= 20\ \mu$m
free wavelength λ	$= 1\ \mu$m
relative index difference Δ	$= 1$ percent
core refractive index n_1	$= 1.46$.

Trapped modes to the right of this line have a loss ratio α_j/χ larger than 1 dB/km. Their number represents approximately a fraction

$$\eta_j \approx \frac{1}{2\pi}\frac{a^2}{s^2v^3}\frac{\ln^3\,(1/a\alpha_j)}{\ln\,(1 + s/a)} \tag{36}$$

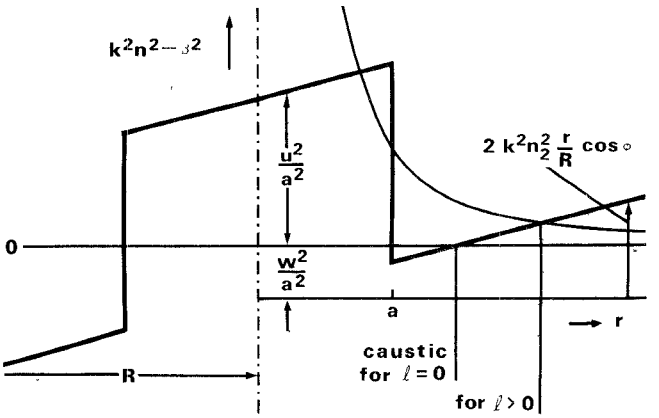

Fig. 9. Equivalent dielectric profile of curved step index fiber; center of curvature is far left (outside field of view) at distance R from guide axis.

of the total mode volume. For the parameters listed above, η_j amounts to about 6 percent. As a rule of thumb, the cladding thickness should be

$$s \approx 36a\eta_j^{-1/2}v^{-3/2} \tag{37}$$

for $\alpha_j/\chi = 1$ dB/km to be restricted to a fraction η_j of all modes. The same relationship holds for the membrane length in the case of the single-material fiber (Fig. 7(b)). The core-membrane structure is typically surrounded by a tube of the same material as core and membranes. This tube provides strength and stiffness and the necessary shield against contamination of the core surface. Naturally, in this case, χ obeys a relationship different from (32).

The bending of a dielectric waveguide produces a source of radiation loss in the cladding; Marcatili and Miller [29] explain this phenomenon as follows: to maintain a guided mode field with equiphase fronts on radial planes, a fraction of the mode field on the outside of the bend would have to exceed the plane wave velocity in the cladding medium. Since this is impossible, the energy associated with this part of the mode field is lost to radiation. For the purpose of evaluating this effect, we reduce the problem to that of a straight guide by conformal mapping [20]; the result is the index distribution shown in Fig. 9. It is easy to convince oneself that the index slope of Fig. 9 causes very nearly the same phase velocity differences as a bend with its center at a large distance R to the left of the profile center. It is also evident that the incessant increase of the index towards the right eventually creates a real radial wave vector component in the cladding, and, as a result, periodic field solutions and a radiative power flow extending to infinity.

Because of the absence of circular symmetry, the field solutions with the profile of Fig. 9 are not of the form (2) or (A9). This fact greatly complicates an estimation of the radiative loss and has limited most published work to the lowest mode orders. Reference [29] is an excellent survey of the literature. The following remarks add some recent results applicable to aribtrary mode orders [30].

As Fig. 9 indicates, the extent of the evanescent field (between the interface and the caustic at which the field turns radiative) increases with increasing azimuthal mode order l. As a result and because of the rapid decay of the evasescent field, meridional mode orders suffer more loss in fiber bends than corresponding azimuthal orders. Furthermore, modes that are degenerate in the straight fiber exhibit differences in loss if they differ in orientation with respect to the plane of curvature: fields that are even or symmetric with respect to this plane behave differently from fields that are odd. The following results are based on WKBJ field solutions for the profile of Fig. 9 expressed in parabolic cylinder coordinates [30]. The power loss per unit length in decibels is

$$\alpha_c = \frac{4.34}{a^2 n_2 k} j_l \frac{w^2}{v^2} (4w^2 + \zeta^{4/3} B^{-1/3,1/2}) \cdot \exp^{-1} (w^2 B^{2/3} + \zeta^{2/3} - \tfrac{4}{3} B^{-1/3})^{3/2} \quad (38)$$

with

$$B = \frac{2}{3} \frac{R}{n_2^2 k^2 a^3} \quad (39)$$

and

$$\zeta = \pi \begin{cases} l + \tfrac{1}{2}, & \text{for even modes} \\ l, & \text{for odd modes.} \end{cases} \quad (40)$$

In the case of the single-mode fiber operated at $v = 2$, the first term in the exponential of (38) dominates. For $\alpha_c = 1$ dB/km, we obtain with the help of the parameters of Fig. 2

$$R = (5 + 0.2 \ln \Delta) \lambda \Delta^{-3/2}. \quad (41)$$

A relative index difference of 0.3 percent corresponds to a core diameter of 5.6 μm and permits a bending radius of 23 mm, which is in the vicinity of the mechanically safe bending limit.

The line $\alpha_c = 1$ dB/km in Fig. 8 represents a computation of the bending loss on the basis of (38) for the fiber characterized earlier and bent to a radius of 15 mm. In general, the fraction of modes having a loss α_c larger than 1 dB/km is approximately

$$\eta_c = 0.1 \frac{[\frac{4}{3} B^{-1/3} + \ln^{2/3} (\Delta^{1/2} a \alpha_c)]^{5/2}}{v \Delta (R k n_2)^{2/3}}. \quad (42)$$

For the example above, $\eta_c = 8$ percent.

So far, we have ignored modes outside the cutoff line denoted by $u = v$ in Fig. 8. For these modes, the zero level in Fig. 4(a) falls below the cladding level $k^2 n_2^2 - \beta^2$. This implies radiative field solutions throughout the cladding and intolerable loss if $l = 0$. For $l \neq 0$, however, the radiative field solutions exist only beyond the caustic at $r = al(u^2 - v^2)^{-1/2}$, where the function l^2/r^2 in Fig. 4 intersects the level $k^2 n_2^2 - \beta^2$. For large l, leakage through the evanescent field region between the interface and the caustic is small [31], and hence these modes can propagate long distances even though $u > v$. To obtain a simple estimate, we make the assumption that $u^2 - v^2 \ll l^2$, because this condition permits the largest extent of the evanescent field region and thus promises the least leakage. For typical multimode fibers for long-distance transmission which have $v < 50$, this is a valid approximation, since the loss of modes not fulfilling this condition is so high that they are of no further interest. Similar power flow considerations as for the jacket problem lead to the loss coefficient [31]

$$\alpha_l = 4.34 \frac{l - 1}{a^2 \beta} \left(1.85 \frac{u^2 - v^2}{l^2 - 1} \right)^l. \quad (43)$$

The line $\alpha_l = 1$ dB/km in Fig. 8 depicts the result for the parameters listed earlier. Modes to the left of this line must be considered as propagating even though they are theoretically "cut off." The relative increment in mode volume as a result of these modes is approximately

$$\eta_l = 0.1 (a \alpha_l / \Delta^{1/2})^{1/v}. \quad (44)$$

This result holds for $v < 50$, a condition that seems to be fulfilled for typical multimode fibers envisaged in optical communication applications. The fiber characterized earlier has $\eta_l = 6$ percent.

It is interesting to note that the last three loss processes (α_j, α_c, and α_l), which all originate from some form of leakage through the evanescent field region, show a sharp rise of loss at a certain mode order. This permitted us to define this effect in terms of a reduction of the total mode volume rather than as a loss per unit length. If the leaky modes are not excited and coupling is absent, a loss based on these effects should essentially be avoidable. As we shall see, it is the presence of coupling which turns these effects into an actual loss per unit length.

Mode coupling is caused predominantly by perturbations which have a periodicity in propagation direction equal to the beat wavelength Λ pertaining to the two modes that are coupled [32]. This wavelength is the distance within which the phase of one of the modes lags a total of 2π behind the other.The phase lag per unit length is

$$\kappa = \frac{2\pi}{\Lambda} = \left| \frac{\partial \beta}{\partial m} dm + \frac{\partial \beta}{\partial l} dl \right| \quad (45)$$

where $dm = 0, \pm 1, \pm 2, \cdots$ and $dl = 0, \pm 1, \pm 2, \cdots$ are the differences in the order numbers between the two modes. With the help of (15), we obtain, for example,

$$\kappa = \frac{\tan \theta}{a} \frac{dm\pi + dl \arccos (l/u)}{(1 - l^2/u^2)^{1/2}} \quad (46)$$

for the classical uniform core index. Most perturbations are random and of a kind which strongly favors coupling between neighboring modes having a long beat wave-

length or small κ. The combinations $dm = 0, \pm 1$ and $dl = 0, \pm 1$ are therefore of particular importance. Moreover, the nature of the perturbation excludes certain transitions; directional changes of the guide axis, for example, permit only $dl = \pm 1$. Even with these restrictions, the κ-values of neighboring modes of the cylindrical step-index, as obtained from (46), are functions of m and l that are too complicated for a rigorous evaluation of mode coupling in a multimode fiber. All studies so far have therefore used approximations for the κ-values similar to the one obtainable by applying (45) to (21). In that case, if $g \rightarrow \infty$, the minimum κ-value between neighboring modes is

$$\bar{\kappa} = \frac{u}{\beta a^2} = \frac{\tan \theta}{a} \tag{47}$$

for the uniform core.

As an important source of mode coupling, let us consider the effect of random directional changes of the axis of a multimode fiber of the classical type (uniform core). We assume that we know the "power spectrum" $\Phi(\kappa)$ of the curvature. The power coupling coefficient pertaining to two modes with phase lag $\bar{\kappa}$ is then

$$C = \tfrac{1}{4}\Phi(\kappa)\,(akn_1)^2 = \Phi v^2/8\Delta. \tag{48}$$

Because of our approximation (47), C is a function of u only and not explicitely of m and l. To simplify our problem even further, we assume that also the loss distribution, which may be caused by a combination of the loss phenomena discussed earlier, is only a function of u. We therefore write it as $\alpha(u)$. In that case, the transition to a mode continuum permits us to reduce the coupling among all M modes to some form of diffusion phenomenon governed by a partial differential equation of the form [34]

$$\frac{\partial}{\partial u}\left(C\frac{\partial Q}{\partial u}\right) = \alpha(u)\frac{\partial Q}{\partial z}. \tag{49}$$

where $Q(u)$ is the power distribution in the mode groups characterized by u.

No matter what power distribution is excited at the fiber input, coupling and the loss processes involved eventually establish a dynamic equilibrium which transforms $Q(u)$ into a distribution $P(u)$, such that $Q = P \exp(-Az)$, where P is the lowest eigenfunction and A the lowest eigenvalue of (49). In other words, the power distribution assumes a function which minimizes the loss A. Equation (49) then becomes

$$\frac{\partial}{\partial u}\left(C\frac{\partial P}{\partial u}\right) = [\alpha(u) - A]P. \tag{50}$$

Note that $P(u)$ is the far-field power density discussed earlier in the limit that $ka \rightarrow \infty$.

A good phenomenological description of measured results [35], [36, fig. 5] which leads to the Poschl–Teller differential equation [22], [37] is provided by

$$\alpha(u) = \epsilon \tan^2 \frac{\pi}{2}\frac{u}{v}. \tag{51}$$

For this loss distribution and if we assume $\Phi(\bar{\kappa}) = \Phi_c$ to be independent of $\bar{\kappa}$, the lowest eigenvalue A of (50) obeys the relation

$$\Phi_c = \frac{2\Delta A}{1 + \epsilon/A}. \tag{52}$$

One of the best fibers made to date had for example [35], [36], $\Delta = 1$ percent and $\epsilon \approx A \approx 1$ dB/km; hence $\Phi_c = 0.0023$ km^{-1}. The results do not change significantly if Φ, rather than being independent of $\bar{\kappa}$, is a slowly decreasing function of κ with $\Phi_c = \Phi(\bar{\kappa}_{\max})$. To understand the physical significance of the value obtained for Φ_c, let us assume that Φ results from a number of minor, but relatively abrupt, directional changes distributed randomly over 1 km of fiber length. Let the directional change be 0.1 degree of angle occurring within 0.1 mm of fiber length (radius of curvature 57 mm). In that case, 76 directional changes per kilometer are sufficient to cause the value Φ_c obtained above. Note that it is the change of curvature, not curvature itself, which produces coupling and coupling loss. As noted earlier, a much stronger, but constant curvature of 15 mm radius produces an elimination of some high-order modes, but essentially no loss, if these modes are not excited and coupling is abscent.

A study of the parabolic profile for the case $\epsilon = 0$ (abrupt loss increase at $u = v$) can be found in [38]. In that case, $\bar{\kappa} = \bar{\kappa}_{\max}$ for all modes so that only $\Phi(\bar{\kappa}_{\max})$ must be considered. It leads essentially to the relation (52) with $\epsilon = 0$.

IV. DELAY DISTORTION

A number of promising applications of fibers are in communication systems which utilize some form of digital envelope modulation of the optical signal [5]. Accordingly, fiber performance is usually characterized in terms of the degradation of an optical pulse propagating through the fiber. We shall follow this practice; alternative descriptions like the baseband frequency characteristic of the fiber can, at least in principle, be obtained from the above results by a simple Fourier transformation [39]. The delay per unit length of a light pulse at a given carrier frequency f_0 is

$$t = \frac{1}{c}\frac{d\beta}{dk}\bigg|_{f=f_0}. \tag{53}$$

If the carrier has a spectral width B which is broad compared to that of the detected pulse envelope, the pulse spread per unit fiber length as a result of the change of $d\beta/dk$ with f is approximately [40]

$$\tau = \frac{1}{c}\frac{B}{f_0}k\frac{d^2\beta}{dk^2}\bigg|_{f=f_0}. \tag{54}$$

The propagation constant β is a function of k, not only because the index changes with frequency (material dispersion), but, in addition, because β in (5) is a function of the v-value which in turn is proportional to frequency. This effect is here called "waveguide dispersion." A third pulse impairment is a consequence of the fact that (53) is a function of the mode number, so that a pulse spread arises in multimode fibers even if the frequency dependence is neglected.

As far as their effect on the signal is concerned, material and waveguide dispersion are interrelated in a complicated way; however, by computing one in the absence of the other, we can show that the material effect usually dominates and the waveguide effect can be neglected. We assume first that the carrier is a plane wave propagating in a dielectric of index $n(f)$. We have $\beta = nk$ and, since $dk/k = df/f = -d\lambda/\lambda$, we obtain from (54)

$$\tau = \frac{1}{c}\frac{B}{f_0}\lambda^2 \frac{d^2n}{d\lambda^2}\bigg|_{\lambda=c/f_0}. \tag{55}$$

The coefficient $\lambda^2 d^2n/d\lambda^2$ computed from index data of a silica-rich core material [41] is plotted in Fig. 10. Also shown is the result of a direct measurement of the effect [42] at a wavelength of 0.8 μm. Typical luminescent diodes made from Al–Ga–As have a spectral width (between $1/e$ points) of 4 percent and hence produce a τ of 4 ns/km when operated at 0.8 μm [43]. The effect could be substantially reduced, if such sources could be operated at longer wavelengths, possibly by using In–Ga–As instead of Al–Ga–As [44].

Next consider a classical (step-index) fiber made from a dispersionless material. To calculate $d\beta/dk$, we write (30) in the form

$$\frac{\beta}{k}\frac{d\beta}{dk} = n_1^2\frac{P_1}{P} + n_2^2\frac{P_2}{P} \tag{56}$$

and obtain with the help of (4) and (6)

$$\frac{d\beta}{dk} = \frac{1}{\beta k}\left[\beta^2 + \frac{w^2}{a^2}j_1\right] \approx n_2 + (n_1 - n_2)\frac{w^2}{v^2}(1 + 2j_1). \tag{57}$$

In order to compare this with the coefficient in Fig. 10, we have plotted

$$(n_1 - n_2)^{-1} k d^2\beta/dk^2 \tag{58}$$

as obtained from (57) for the fundamental mode versus v in Fig. 2. The coefficient reaches a maximum at $v = 1.2$, but decreases to about 0.28 at a typical operating point of $v = 2$. Thus $kd^2\beta/dk^2 = 0.4$ to 0.04 percent for $\Delta = 1$ to 0.1 percent, as compared to $\lambda^2 d^2n/d\lambda^2 = 3.1$ percent at 0.8 μm wavelength.

Waveguide dispersion coefficients as high as those indicated in Fig. 2 occur in multimode fibers only for those

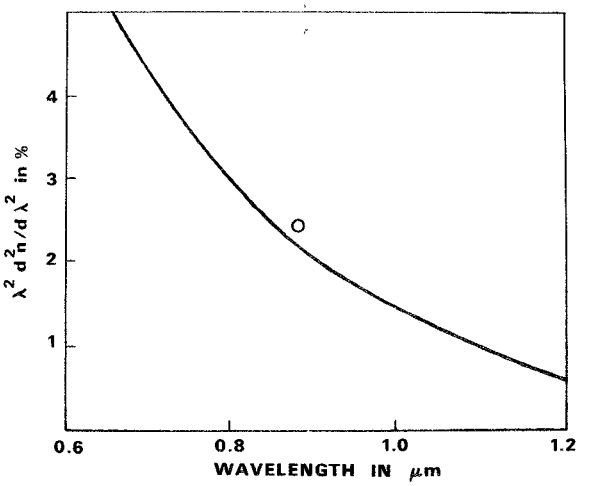

Fig. 10. Material dispersion coefficient for silica-rich core [41] plotted versus wavelength. Dot indicates measured value [42].

modes which are operated relatively close to cutoff. Even if these modes are fully transmitted, they constitute a sufficiently small number to have little influence on the pulse distortion as far as their waveguide dispersion is concerned. In these fibers, it is the delay difference between individual modes which distorts the pulse.

To study this effect, we introduce (17) into (57) and write

$$\frac{d\beta}{dk} = \frac{n_1^2 k}{\beta}\left[1 - \frac{u^2}{v^2}\frac{2\Delta}{h + (w^2 + l^2)^{1/2}}\right]. \tag{59}$$

The term $n_1^2 k/\beta$ is easily identified as the ray-optics approximation for $d\beta/dk$. As a mode approaches cutoff, w and l can be small enough to reduce the ray optics delay $n_1^2 k/\beta$ by a significant amount, producing what is known in the slab structure as the Goos–Haenchen shift [9], [45]. In fact, for $l = 0$, this shift coincides exactly with that of the TE slab modes [45]. Most modes in multimode fibers propagate sufficiently far from cutoff that $n_1^2 k/\beta$ is a satisfactory approximation for all. Let us now estimate the magnitude of these delays directly for the general class of graded profiles (20), of which the classic step-index profile is a special member. We use (21) and (53) to find [23]

$$t(u) = \frac{n_0^2 k}{c\beta}\left(1 - \frac{4\Delta}{g + 2}\frac{u^2}{v^2}\right) \tag{60}$$

which reduces to $n_0^2 k/c\beta$ for $g \to \infty$. For arbitrary g, the delay of the mode of lowest order is $t(0) = n_0/c$. The highest orders have $u = v$ and $t(v) = (n_0/c)(1 - 2\Delta)^{1/2}$. The maximum difference is therefore $t_{max} - t_{min} \approx n_0\Delta/c$ for $g \to \infty$. If $\Delta = 1$ percent this amounts to about 50 ns/km.

Optimal equalization occurs for [23]

$$g = 2 - 2\Delta \tag{61}$$

which characterizes a profile very close to the parabolic. In that case $t(0) = t(v) = n_0/c$, but all other modes have

$t(u) < n_0/c$, the fastest arriving at $t(v/\sqrt{2}) = n_0\Delta^2/8c$. For arbitrary g, the delay difference between the slowest and the fastest mode is

$$t_{max} - t_{min} = \frac{n_0}{c} \begin{cases} \Delta(g - 2 + 2\Delta)/(g + 2), & 2 < g \\ (g - 2 + 4\Delta)^2/32, & 2 - 2\Delta < g < 2 \\ (g - 2)^2/32, & 2 - 4\Delta < g < 2 - 2\Delta \\ \Delta(2 - 2\Delta - g)/(g + 2), & 1 < g < 2 - 4\Delta. \end{cases} \quad (62)$$

Evidently, good equalization occurs in a very narrow region of g values and requires accurate control of the grading process during the fiber or preform preparation. That these requirements can be met very closely was demonstrated by the early Selfoc fibers [46], whose profile had a g-value of very nearly $2 - \Delta$ in a large part of the cross section [47]; experiments proved that these fibers showed indeed an amazingly good mode equalization [48]. For those profiles, which belong to the class (20), but whose g-values deviate from the optimal, we can calculate the maximum delay spread as a function of the maximum deviation dn of the index from the optimal anywhere between $r = 0$ and $r = a$. The ratio $dn/n_0\Delta$ is called the profile error; we use it as a parameter in Fig. 11. Plotted in Fig. 11 is the index difference or the numerical aperture which would lead to a given delay spread per kilometer for various profile errors. Also shown is the spread caused by material dispersion in silica fibers, when the carrier source is an Al–Ga–As luminescent diode operated at 0.8 μm.

Equation (62) must be considered as an upper bound for the pulse broadening possible as a result of mode delay differences. The actual broadening is usually much smaller; two effects are responsible for this. One is the selective loss of certain modes or mode groups as a result of the loss effects discussed in Section III. The other is mode coupling which tends to average the delay by "switching the light around" among the various modes. To study the first effect, consider the example of a graded-index fiber whose material loss varies in the fiber cross section according to the relation (31). The reason for such a variation was explained earlier. Let us exclude the singularity in the vicinity of the parabolic distribution for the time being and assume that the g-value of our fiber deviates substantially from 2. A profile error of 10 percent, for example, corresponds approximately to $g = 3$. If the material loss were the same everywhere and all modes were excited equally, the arrival of all modes at the end of a transmission path L would fall into the interval

$$Ln_0/c < T < (Ln_0/c)\,\Delta(g - 2)/(g + 2),$$

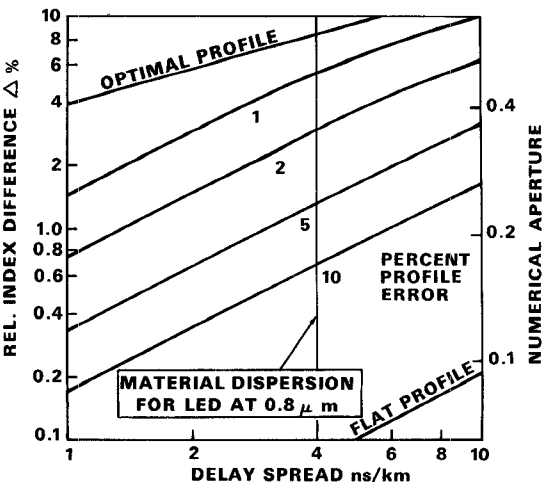

Fig. 11. Relative index difference Δ and numerical aperture which produce delay spread plotted along absissa for various profile errors $dn/n_0\Delta$.

where T is related to the mode parameter u by [23]

$$T(u) = \frac{n_0 L}{c}\,\Delta\,\frac{g - 2}{g + 2}\,\frac{u^2}{v^2}. \quad (63)$$

The power density per unit time interval would be proportional [23] to $T^{2/g}$. If the two loss values α_0 and α_2 of (28) are different, we find the loss as a function of u from (31), and using (63), can write the power distribution as proportional to

$$T^{2/g} \exp\left[-0.46(\alpha_2 - \alpha_0)cT/n_0\Delta(g - 2)\right]. \quad (64)$$

with α_0 and α_2 in dB/km. The rms value of this distribution is

$$\sigma = \frac{n_0\Delta}{c}\,\frac{(1 - 2/g)\,(1 + 2/g)^{1/2}}{0.86g(\alpha_2 - \alpha_0)} \quad (65)$$

as long as $\sigma \ll T(v)$ of (63). The rms value is a good measure of the expected pulse broadening and of the limits of the information rate of transmission [49]. Note that (65) is independent of the transmission distance L. As an example, let us assume $\alpha_0 = 20$ dB/km, $\alpha_2 = 40$ dB/km, $\Delta = 1$ percent, and $g = 3$. As long as $L > 2$ km, the rms width can approximately be computed from (63) using $T^{2/g}$ as the power distribution. One finds an rms value of 2.8 ns/km. For $L > 2$ km, (65) applies and the rms width asymptotically approaches a value of 3.5 ns. This obviously desirable limitation of the pulse broadening is achieved by extinguishing some of the high-order modes. If these modes represent a necessary and important part of the carrier as in the case of an incoherent source, the overall loss resulting from this extinction may represent an intolerable penalty payed for the improvement in signal distortion. For the example discussed earlier, this penalty is 19 dB after 4 km. At that point, the rms value of 3.5 ns is about 3 times shorter than that expected without mode-dependent loss.

Mode coupling produces a similar signal improvement [50]. In fact, all by itself and if limited to trapped modes, it achieves this improvement without a loss penalty. In practice, the influence of mode coupling is difficult to separate from the loss effects. In the presence of both, the signal improvement as well as the loss penalty are complicated functions of the interdependence of coupling and loss in the various modes [51]. So far only the simplest models have been considered. A convenient treatment of the problem begins with (49) considering the time dependence of $Q(u,T,z)$ by an additional term $t(u)\partial Q/\partial T$ with t from (60) and $\partial Q/\partial T$ being the partial derivative with respect to time. Closed-form solutions of the resulting partial differential equation have been given only for the step-index profile, large ϵ in (51) and $C(u)$ = constant [52]. However, it can be shown [50]–[52] that, for a transmission length $L \gg \Delta/C(v)$, when the dynamic equilibrium distribution is established, the power output becomes a Gaussian in time, whose rms value σ increases as $L^{1/2}$. This relation obtains under a wide variety of conditions independent of specific fiber characteristics. The loss penalty is then equal to 4.34 AL in dB with A being the equilibrium loss coefficient obtained from (50). Let σ_0 be the rms width of the output power distribution in the absence of coupling and (mode-dependent) loss. Since σ_0 is proportional to L, the product

$$G = 4.34 \left(\frac{\sigma}{\sigma_0}\right)^2 AL \text{ in dB} \tag{66}$$

is independent of L and has come to be used as the figure of merit of a given (or artifically introduced) combination of coupling and loss.

The most desirable loss distribution would be described by a small coefficient ϵ in (51), leading to a sharp increase of $\alpha(u)$ at $u = v$, which accounts for the transition from trapped to leaky modes. Most discussions of the problem therefore consider a first approximation with $\epsilon = 0$. A variety of coupling functions $C(u)$ have been considered, among them the class [53]

$$C(u) = C(v)\,(v/u)^p. \tag{67}$$

To summarize the results, Fig. 12 presents a plot of $G(z)$ for $\epsilon = 0$ and a uniform core index. The figure of merit of the parabolically graded fiber [38] with $\epsilon = 0$ is $G = 0.27$.

V. CONCLUSIONS

We have tried to give a consistent picture of the theory of the optical fiber, as far as it is most relevant to design and systems questions in optical transmission applications. In most cases, we have opted for clarity and simplicity rather than utmost accuracy and hope that those interested in better accuracy can find it in the references cited. The main approximation underlying all problems discussed here is the assumption of essentially forward directed propagation and, following from that, transverse electromagnetic field solutions. We have used the WKBJ approach for all multimode fibers, even in the case of a uniform core index, because it provides a clear mode picture, a simple correspondence between modes and rays and an effortless transition to a mode continuum. In addition, it is easily extendable to graded-index profiles. Higher order approximations extending beyond the paraxial results are obtained where necessary, as, for example, in the computation of the group delay for near-parabolic profiles. Emphasis was placed on those characteristics of fibers, which deviate significantly from those of slab or film guides; this is particularly important for multimode fibers which transmit a large number of modes with high azimuthal orders. Practical aspects of fiber design, as, for example, the influence of a finite cladding width, curvature, cross sectional loss variations, material dispersion, and the effect of index profile tolerances were assessed. The large variety of potential applications made it unpractical to consider specific designs; we hope that the results are presented in a sufficiently simple way so that the reader can use them to solve his specific problems.

APPENDIX

WKBJ APPROXIMATIONS FOR CYLINDRICAL STRUCTURES

The general wave equation becomes separable in a cylindrical coordinate system (r,ϕ,z), if the refractive index n is a function of r only. In that case, the differential equation for the radial field dependence $E(r)$ assumes the form

$$\frac{\partial^2 E}{\partial r^2} + \frac{1}{r}\frac{\partial E}{\partial r} + \left[k^2 n^2(r) - \beta^2 - \frac{l^2}{r^2}\right] E = 0. \tag{A1}$$

We set

$$E = F \exp\left[ikS(r)\right] \tag{A2}$$

where F is a coefficient independent of r. Upon substitution into (A1), we have

$$ikS'' + (ikS')^2 + ikS'/r + (k^2n^2 - \beta^2 - l^2/r^2) = 0 \tag{A3}$$

where the primes denote differentiation with respect to r. We now assume that n changes slowly within a distance comparable to the wavelength λ, so that an expansion of $S(r)$ in powers of λ converges rapidly. (For the classical structure, we exclude the area around the index step; the step can later be accounted for by suitable matching conditions.) After substituting

$$S(r) = S_0 + \frac{1}{k} S_1 + \cdots \tag{A4}$$

into (A3) and equating equal powers of λ, one obtains the

following equations for the first two terms of the expansion (A4):

$$-(kS_0')^2 + (k^2n^2 - \beta^2 - l^2/r^2) = 0 \qquad \text{(A5)}$$

$$ikS_0'' - 2kS_0'S_1' + ikS_0'/r = 0. \qquad \text{(A6)}$$

Integration of these equations yields

$$S_0 = \pm \int^r (n^2 - \beta^2/k^2 - l^2/k^2r^2)^{1/2}\, dr \qquad \text{(A7)}$$

and

$$S_1 = (i/4) \ln (r^2n^2 - \beta^2r^2/k^2 - l^2/k^2) \qquad \text{(A8)}$$

plus constants of integration which are omitted for clarity. In order to construct the complete solutions, we have to distinguish between three regions (see Fig. 4 or 6): the tube in which propagating field conditions obtain (S_0 real), and the two regions inside and outside of that tube in which S_0 is imaginary.

Let us consider the classical index distribution of Fig. 4 as an example. In the case of lossless propagation, standing-wave conditions obtain for the cross sectional field distribution in the propagation region. Hence, in order to obtain a solution of the form $\cos(kS_0 + \psi)$, we must consider both signs of (A7) in this region. The phase term ψ is determined by the matching conditions at the inner caustic. In the case of the classical structure, we have [20] $\psi = -\pi/4$. The field outside the propagation region vanishes for $r \to \infty$. We therefore choose the sign in (A7) to produce a decaying exponential for increasing r. To obtain the field solutions in the propgation region ($n = n_1$) and in the cladding region ($n = n_2$), we use the abbreviations (9) and (10) in (A8) and (A9), insert the latter equations into (A4) and finally write (A2) with the help of (A4) in the form

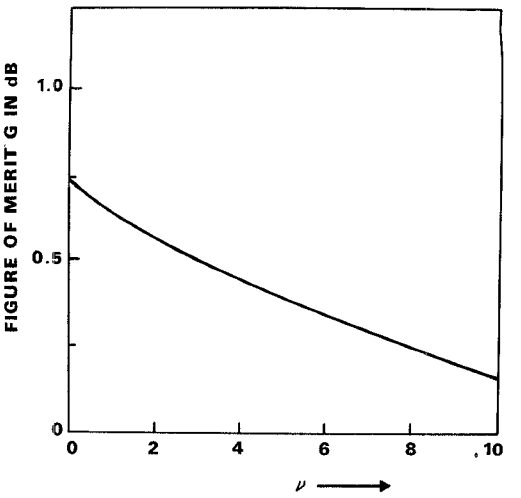

Fig. 12. Figure of merit $G(\nu)$ for coupling coefficients proportional to $(u/v)^\nu$, for $\epsilon = 0$ (abrupt loss increase at $u = 0$), and a step-index profile.

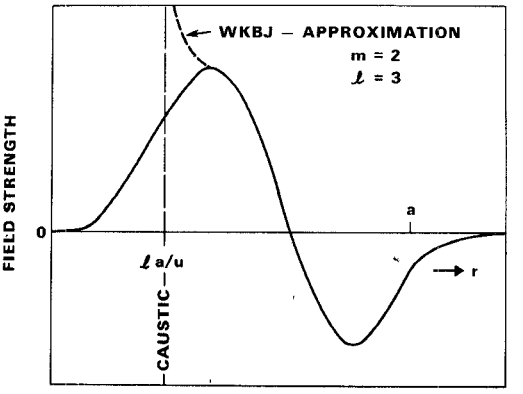

Fig. 13. Transverse mode field for $m = 2$ and $l = 3$ (solid line). WKBJ approximation coincides with exact solution everywhere except as shown by dashed line.

$$E(r) = \begin{cases} F_1(2a/\pi\hat{u}r)^{1/2} \cos\left[-\frac{\pi}{4} + \int_{al/u}^{r} \hat{u}\, dr/a\right] & \frac{al}{u} < r < a \\ F_2(\pi a/2\hat{w}r)^{1/2} \exp\left[-\int_{a}^{r} \hat{w}\, dr/a\right] & r > a \end{cases} \qquad \text{(A9)}$$

where the constants F_1 and F_2 have been chosen such that the solutions coincide with the Debye approximations of the Bessel functions $J_l(ur/a)$ and $K_l(wr/a)$, respectively [19]. They describe the Bessel functions with surprising accuracy even to the lowest order numbers. Fig. 13 illustrates the example $m = 2$, $l = 3$.

Just as in the case of the more accurate solution (2), the relations between u and w and between F_1 and F_2 are obtained from the match of the field solutions (A9) and their radial derivatives at $r = a$. However, a satisfactory solution for the majority of the modes of a multimode fiber is based on the assumption $F_2 = 0$ which ignores the evanescent fields altogether. In this case, propagating modes exist [20], [22] when

$$\int_{la/u}^{a} \hat{u}\, dr/a = (m - \tfrac{1}{4})\pi \qquad \text{(A10)}$$

where $m = 1,2,\cdots$ is the meridional order number. As the $\pi/4$-term on the right is significant only for a few low-order modes, it is neglected in the text.

ACKNOWLEDGMENT

The author wishes to thank D. Marcuse for helpful discussions.

REFERENCES

[1] R. D. Maurer, "Glass fibers for optical communications," *Proc. IEEE*, vol. 61, pp. 452–462, Apr. 1973.

[2] M. M. Ramsay, "Fiber optical communications within the United Kingdom," *Opto-Electron.*, vol. 5, pp. 261–274, July 1973.

[3] S. Maslowski, "Activities in fiber-optical communications in Germany," *Opto-Electron.*, vol. 5, pp. 275–284, July 1973.

[4] H. Ohnesorge, "Neue Möglichkeiten fur Nachrichtensysteme auf der Basis des Laser-Glasfaserkanals," Nachrichtentech. Rep. 17, Berlin, 1973.

[5] S. E. Miller, E. A. J. Marcatili, and T. Li, "Research toward optical-fiber transmission systems," *Proc. IEEE*, vol. 61, pp. 1703–1725, Dec. 1973.

[6] R. A. Andrews, A. F. Milton, and T. G. Giallorenzi, "Military applications of fiber optics and integrated optics," *IEEE Trans. Microwave Theory Tech. (1973 Symposium Issue)*, vol. MTT-21, pp. 763–769, Dec. 1973.

[7] N. S. Kapany, *Fiber Optics*. New York: Academic, 1967.

[8] D. Gloge, "Optical fibers for communication," *Appl. Opt.*, vol. 13, pp. 249–254, Feb. 1974.

[9] N. J. Kapany and J. J. Burke, *Optical Waveguides*. New York: Academic, 1972.

[10] D. Marcuse, *Light Transmission Optics*. New York: Van Nostrand, 1972.

[11] ——, *Theory of Dielectric Optical Waveguides*. New York: Academic, 1974.

[12] T. Uchida, "Progress of optical fibers and optical integrated circuits in Japan," presented at the 1973 Conf. Laser Engineering and Application, Washington, D. C. (Abstract in *IEEE J. Quantum Electron.*, vol. QE-9, p. 687, June 1973.)

[13] S. E. Miller, "Light propagation in generalized lens-like media," *Bell Syst. Tech. J.*, vol. 44, pp. 2017–2064, Nov. 1965.

[14] P. Kaiser, E. A. J. Marcatili, and S. E. Miller, "A new optical fiber," *Bell Syst. Tech. J.*, vol. 52, pp. 265–269, Feb. 1973.

[15] H. Kogelnik and T. Li, "Laser beams and resonators," *Appl. Opt.*, vol. 5, pp. 1550–1567, Oct. 1966.

[16] A. W. Snyder, "Asymptotic expressions for eigenfunctions and eigenvalues of a dielectric or optical waveguide," *IEEE Trans. Microwave Theory Tech. (1969 Symposium Issue)*, vol. MTT-17, pp. 1130–1138, Dec. 1969.

[17] D. Gloge, "Weakly guiding fibers," *Appl. Opt.*, vol. 10, pp. 2252–2258, Oct. 1971.

[18] M. B. Panish, "Heterostructure injection lasers," this issue, pp. 20–30.

[19] M. Abramowitz and I. A. Stegun, *Handbook of Mathematical Functions*. New York: Dover, 1964, p. 366.

[20] S. J. Maurer and L. B. Felsen, "Ray methods for trapped and slightly leaky modes in multilayered or multiwave regions," *IEEE Trans. Microwave Theory Tech.*, vol. MTT-18, pp. 584–595, Sept. 1970.

[21] C. N. Kurtz and W. Streifer, "Guided waves in inhomogeneous focusing media," *IEEE Trans. Microwave Theory Tech.*, vol. MTT-17, pp. 250–263, May 1969.

[22] J. P. Gordon, "Optics of general guiding media," *Bell Syst. Tech. J.*, vol. 45, pp. 321–332, Feb. 1966.

[23] D. Gloge and E. A. J. Marcatili, "Multimode theory of graded-core fibers," *Bell Syst. Tech. J.*, vol. 52, pp. 1563–1578, Nov. 1973.

[24] E. A. J. Marcatili, "Slab-coupled waveguides," *Bell Syst. Tech. J.*, vol. 4, pp. 645–674, Apr. 1974.

[25] W. A. Gambling, D. N. Payne, and Y. Matsumura, "Gigahertz bandwidths in multimode, liquid-core, optical fiber waveguide," *Opt. Commun.*, vol. 6, pp. 317–322, Dec. 1972.

[26] K. M. Case, "On wave propagation in inhomogeneous media," *J. Math. Phys.*, vol. 13, p. 360, 1972.

[27] D. Marcuse, "The coupling of degenerate modes in two parallel dielectric waveguides," *Bell Syst. Tech. J.*, vol. 50, pp. 1791–1816, July–Aug. 1971.

[28] E. A. J. Marcatili and S. E. Miller, "Improved relations describing directional control in electromagnetic wave guidance," *Bell Syst. Tech. J.*, vol. 48, pp. 2161–2187, Sept. 1969.

[29] E. G. Neumann and H. D. Rudolph, "Radiation from bends in dielectric rod transmission lines," this issue, pp. 142–149.

[30] D. Gloge, "Mode fields and loss in curved fibers," unpublished work.

[31] A. W. Snyder and D. J. Mitchell, "Leaky rays cause failure of geometric optics on optical fibers," *Electron. Lett.*, vol. 9, pp. 437–438, Sept. 1973.

[32] S. E. Miller, "Some theory and applications of periodically coupled waves," *Bell Syst. Tech. J.*, vol. 48, pp. 2189–2219, Sept. 1969.

[33] D. Marcuse, "Mode conversion caused by surface imperfections of a dielectric slab waveguide," *Bell Syst. Tech. J.*, vol. 48, pp. 3187–3215, Dec. 1969.

[34] D. Gloge, "Optical power flow in multimode fibers," *Bell Syst. Tech. J.*, vol. 51, pp. 1767–1783, Oct. 1972.

[35] D. B. Keck, R. D. Maurer, and P. C. Schultz, "On the ultimate lower limit of attenuation in glass optical waveguides," *Appl. Phys. Lett.*, vol. 22, pp. 307–309, Apr. 1973.

[36] D. B. Keck, "Spatial and temporal power transfer measurements on a low-loss optical waveguide," *Appl. Opt.*, vol. 13, pp. 1882–1888, Aug. 1974.

[37] G. Pöschl and E. Teller, "Bemerkungen zur Quantenmechanik des Anharmonischen Oszillators," *Z. Phys.*, vol. 83, pp. 143–151, 1933.

[38] D. Marcuse, "Losses and impulse response of a parabolic-index fiber with random bends," *Bell Syst. Tech. J.*, vol. 52, pp. 1423–1437, Oct. 1973.

[39] D. Gloge, E. L. Chinnock, and D. H. Ring, "Direct measurement of the (baseband) frequency response of multimode fibers," *Appl. Opt.*, vol. 11, pp. 1534–1538, July 1972.

[40] R. B. Dyott and J. R. Stern, "Group delay in glass fiber waveguide," *Electron. Lett.*, vol. 7, pp. 82–84, 1971.

[41] R. P. Kapron and D. B. Keck, "Pulse transmission through a dielectric optical waveguide," *Appl. Opt.*, vol. 10, pp. 1519–1523, July 1971.

[42] D. Gloge, E. L. Chinnock, and T. P. Lee, "GaAs twin-laser setup to measure mode and material dispersion in optical fibers," *Appl. Opt.*, vol. 13, pp. 261–263, Feb. 1974.

[43] R. W. Dawson, "Pulse widening in a multimode optical fiber-excited by a pulsed GaAs LED," *Appl. Opt.*, vol. 13, pp. 264–265, Feb. 1974.

[44] C. J. Nuese, R. E. Enstrom, and M. Ettenberg, "Room-temperature laser operation of InGaAs junctions," *Appl. Phys. Lett.*, vol. 24, pp. 83–85, Jan. 1974.

[45] K. Artmann, "Berechnung der Seitenverzerrung des totalreflektierten Strahles," *Ann. Physik*, vol. 2, pp. 87–102, 1948.

[46] T. Uchida *et al.*, "Optical characteristics of a light-focusing fiber guide and its applications," *IEEE J. Quantum Electron.*, vol. QE-6, pp. 606–612, Oct. 1970.

[47] T. Kitano, H. Matsumura, M. Furukawa, and I. Kitano, "Measurements of the fourth-order aberration in a lens-like medium," *IEEE J. Quantum Electron.*, vol. QE-9, pp. 967–971, Oct. 1973.

[48] D. Gloge, E. L. Chinnock, and K. Koizumi, "Study of pulse distortion in Selfoc fibers," *Electron. Lett.*, vol. 8, pp. 526–527, Oct. 1973.

[49] S. D. Personick, "Receiver design for digital fiber optic communication systems," *Bell Syst. Tech. J.*, vol. 52, pp. 843–886, July–Aug. 1973.

[50] ——, "Time dispersion in dielectric waveguide," *Bell Syst. Tech. J.*, vol. 50, pp. 843–859, Mar. 1971.

[51] D. Marcuse, "Pulse propagation in multimode dielectric waveguides," *Bell Syst. Tech. J.*, vol. 51, pp. 1199–1232, July–Aug. 1972.

[52] D. Gloge, "Impulse response of clad optical multimode fibers," *Bell Syst. Tech. J.*, vol. 52, pp. 801–816, July–Aug. 1973.